Rheology of "Wet" Polymer Brushes via Brownian Dynamics Simulation: Steady vs Oscillatory Shear

Patrick S. Doyle, Eric S. G. Shaqfeh, and Alice P. Gast
Department of Chemical Engineering, Stanford University, Stanford, California 94305-5025
(Received 14 August 1996)

The rheology of solvent-filled polymer brushes under steady and oscillatory shear is studied by Brownian dynamics simulation. The flow field is solved self-consistently with the polymer dynamics. We find that under steady flow the brushes are shear thinning in both normal forces and shear viscosity. During oscillatory flow, extreme shear thickening occurs when the ratio of the Weissenberg number to the dimensonless flow frequency $\mathrm{Wi}/\omega \approx 3$. *Shear-induced diffusion* is shown to create this thickening. These findings serve to explain the recent measurements made by Klein *et al.* [Nature **352**, 143 (1991); **370**, 634 (1994); Discuss Faraday Soc. **98**, 173 (1994)]. [S0031-9007(97)02368-5]

PACS numbers: 83.10.Nn, 47.15.Gf, 83.20.Jp

The rheological implications of adsorbed or tethered polymer layers have recently become a subject of wide interest [1–3]. These layers can form the basis for very effective lubrication [4], they can stabilize colloids [5], and recent data suggest that they can also have profound effects on the rheology of colloidal suspensions [6]. Models for these brushes under flow are few and they are developed either under the *assumption* of effective porous medium behavior [7,8] or under flow conditions near equilibrium [8]. It is unclear whether these models adequately account for the intermolecular interactions between brush molecules or for brush elasticity under shearing conditions.

Recently the shortcomings of our physical understanding of the brush-solvent and brush-wall interactions have been brought into focus through the experiments of Klein *et al.* [1,2]. These experiments have shown that the normal forces exerted during the shear flow of brushes can be drastically altered if the brushes are sheared in an oscillatory as opposed to a steady manner. Klein *et al.* [1] have demonstrated that dramatic normal force increases can be induced under the application of oscillatory flow. There are now a host of explanations given in the literature for these normal forces and these include hydrodynamic instabilities [9] and shear flow-induced brush thickening [10,11]. Recent simulations of brushes [3,12] demonstrate normal forces under steady slow shearing which are qualitatively similar to those witnessed by Klein *et al.* [2], however, no substantial velocity dependence of these normal forces was witnessed nor any brush thickening. There have been no studies which definitely demonstrate a mechanism that can explain the shear dependence of brush shear and normal forces under flow. In this Letter we present self-consistent Brownian dynamics simulations, which are capable of accurately simulating *nonequilibrium* brush dynamics. Our findings provide a simple physical interpretation of the experimental measurements of Klein *et al.* [1,2].

Our Brownian dynamics simulation method for single chains is described in a previous publication [13]. In short, we use rigid link Kramers [14] freely draining chains to model the polymers. The beads contain the centers of all forces, both intramolecular and intermolecular, which are exerted on the chains. These include drag from the mean flow, excluded volume (via truncated Lennard-Jones potentials on all beads [15]), Brownian forces, and the tensions in the rigid links which serve to constrain the link length [13]. The magnitude of each Cartesian component of the Brownian force on a bead is selected randomly from the uniform distribution $[-(6kT\zeta/\delta t)^{1/2}, (6kT\zeta/\delta t)^{1/2}]$, where ζ is the drag coefficient, kT is the Boltzmann temperature, and δt is the time step size. The stochastic Brownian forces model collisions of the solvent molecules on the beads and are chosen to satisfy the fluctuation-dissipation theorem. The hydrodynamic drag $\mathbf{F}^h$ on the jth bead is

$$\mathbf{F}^h = \zeta\left[\langle \mathbf{u}(\mathbf{R}_j)\rangle - \frac{d\mathbf{R}_j}{dt}\right], \tag{1}$$

where $\mathbf{R}_j$ is the position of the jth bead (cf. Fig. 1), and $\langle \mathbf{u}(\mathbf{R}_j)\rangle$ is the ensemble averaged solvent velocity at position $\mathbf{R}_j$. Although no explicit hydrodynamic interactions between beads are included, the chains interact through the mean flow since it is calculated in a self-consistent manner as described below.

Figure 1 specifies our problem geometry, namely two bounding parallel plates shearing a single solvent-filled

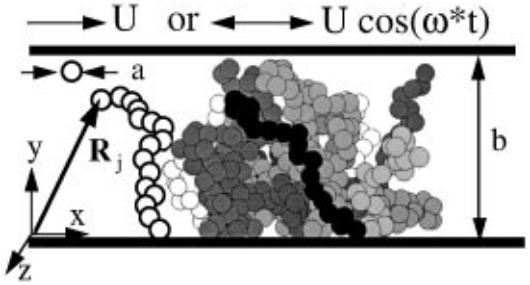

FIG. 1. Schematic of the problem geometry.

 0031-9007/97/78(6)/1182(4)$10.00

brush and gap (via motion of the top plate). The brush is composed of periodically extended rectangular areas containing 20 chains of 20 beads each. The first bead in each chain is randomly placed on the tethering surface ($y = 0$), and the remaining beads perform a self-avoiding random walk. For a given simulation there are four dimensionless parameters which govern the dynamics and flow field: σa^2—the areal fraction of chains where σ is the number/area and a is a bead diameter; $\mathrm{Wi} = U\tau/b$—the Weissenberg number—where τ is the relaxation time of a single isolated chain *in free solution*, U is the upper plate velocity, and b is the gap thickness; $\lambda = b/R_{g0}^{y}$—the dimensionless gap thickness where R_{g0}^{y} is the y component of the radius of gyration of the layer; and, for oscillatory flow, ω—the frequency made dimensionless with τ. All results presented in this Letter are for an areal fraction $\sigma a^2 = 0.125$ (where the simulation box dimensions in the x and z directions are $12.65a \times 12.65a$), and thus well above the overlap areal fraction of $\sigma a^2 = 0.025$ for this system. Furthermore, we will show below that the brushes at this areal fraction are very dense and therefore our assumption that hydrodynamic interactions are screened is a reasonable approximation.

In Eq. (1) the averaged solvent velocity was introduced and needs to be calculated. Under incompressible ($\nabla \cdot \mathbf{u} = 0$) Stokes' flow conditions we can write the general equation for the averaged solvent velocity in the brush as

$$\eta \nabla^2 \langle \mathbf{u} \rangle - \nabla \langle P \rangle + \langle \mathbf{f} \rangle (\mathbf{x}, t; \mathbf{u}) = 0 . \qquad (2)$$

In Eq. (2) η is the solvent viscosity, $\langle P \rangle$ is the averaged solvent pressure, and $\langle \mathbf{f} \rangle$ is the *averaged force density exerted by the brush on the solvent.* The averaged force density $\langle \mathbf{f} \rangle$ is equal to $-\langle \mathbf{F}^h \rho(\mathbf{x}) \rangle$ where $\rho(\mathbf{x})$ is the bead density at position $\mathbf{x}$. We calculate $\langle \mathbf{f} \rangle$ using Eq. (1) and the previous relation. Of course $\langle \mathbf{f} \rangle$ is a functional of the solvent velocity since the dynamics are governed by the solvent flow. This self-consistent mean-field approach for related Brinkman problems has been shown to be a very good approximation [16].

Imposing a steady shear flow in the geometry of Fig. 1, it follows that the averaged solvent velocity reduces to a single scalar x-velocity component $u(y)$ and it is equal to U at $y = b$ (on the top plate) and $u(0) = 0$. The averaged force density $\langle \mathbf{f} \rangle$ has two components, $\langle f_x \rangle$ and $\langle f_y \rangle$, both of which are only functions of y. $\langle f_y \rangle$ serves to alter the solvent pressure and $\langle f_x \rangle$ serves to alter the convective velocity field $u(y)$.

The scheme for our calculations is as follows: A trial velocity and pressure field (usually the Newtonian fields) are chosen and then the Brownian dynamics simulation is completed for a given parameter set. We calculate the ensemble-averages of $\langle f_x \rangle$ and $\langle f_y \rangle$. Discrete forms of these functions are then placed in Eqs. (2), and the velocity fields and pressure fields are calculated numerically using a finite difference scheme. The new velocity field is then employed in the simulations and the iterative process continues until the flow field and the force density $\langle \mathbf{f} \rangle$ are consistent. This procedure usually converges within four iterations. For all runs the Lennard-Jones length scale and the interbead separation was set equal to a, $\zeta = 3\pi\eta a$, $R_{g0}^{y} = 11.5a$, $\tau = 5.7\zeta a^2/kT$, and $\delta t = 5 \times 10^{-5}\tau$.

From these calculations we find that the average values of $d\mathbf{R}_j/dt$ in any y plane are very small. It follows that $\langle f_y \rangle$ is negligible and the solvent pressure is unaffected by the brush. It also follows that the x momentum equation for $u(y)$ becomes a nonlinear Brinkman equation [8,17]. The force density $\langle f_x \rangle$ is now proportional to $\rho(y)u(y)$. Results for the bead density profiles, the resulting hydrodynamic thickness L_h, and the flow profiles are shown in Fig. 2. These density profiles are calculated for a dimensionless gap thickness $\lambda > 1$ and for a range of Weissenberg numbers. In summary, the hydrodynamic thickness remains at its equilibrium plateau value until values of Wi in excess of 0.1, after which the layer thins. The flow makes the brushes more compact though tails in the density profiles are still evident.

In Fig. 3(a) we present our calculations for the normal and shear stress on the walls of the gap as a function of the gap width λ for various Weissenberg numbers. As the gap decreases and we strongly compress the brush the normal forces dramatically increase. Note that at constant Weissenberg number (or alternatively constant shear rate across the gap) the shear forces actually plateau and begin to decrease for small λ. This is also witnessed in the interpretation of these forces as an effective viscosity in Fig. 3(b). For highly compressed brushes the normal forces are larger than the shear forces by two or three orders of magnitude, which is consistent with the measurements of Klein *et al.* [2]. The shear forces are controlled by the length scale over which

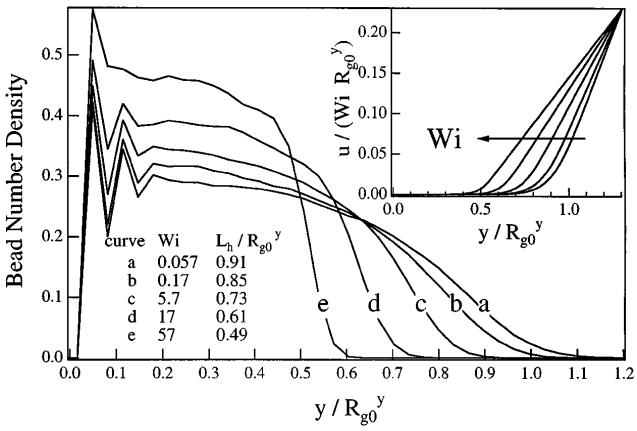

FIG. 2. Bead number density versus distance from tethered surface in steady shear flow. The inset graph shows the self-consistent velocity versus distance from tethered surface and the inset table shows the hydrodynamic thickness L_h.

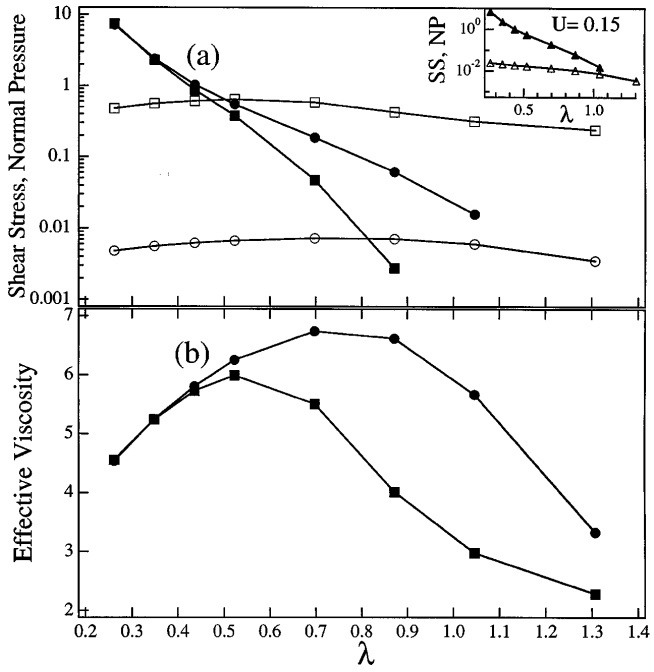

FIG. 3. (a) Shear stress and normal pressure in units (kT/a^3) and (b) effective viscosity in units η versus λ for steady shear flow. The shear stress is shown for Wi = 0.057 (∘) and Wi = 5.7 (□), and the normal pressure for Wi = 0.057 (•) and Wi = 5.7 (■). The inset in (a) shows the shear stress (△) and normal pressure (▲) versus λ for a constant upper plate velocity $U = 0.15$. In (b) the effective viscosity is shown for Wi = 0.057 (•) and Wi = 5.7 (■).

the velocity drops to zero in the solvent/brush region. When the gap thickness is larger than the equilibrium thickness of the brush, the size of this region is controlled by the thickness of solvent above the brush. However, when the brush is physically compressed by the upper plate, then the shear forces are controlled by the effective Brinkman pore size in the layer. Simple geometric scaling arguments show that this pore size decreases like $\lambda^{1/2}$ for decreasing λ. Thus the effective viscosity, at a constant gap shear rate U/b, increases as one first compresses the brush and drives flow through a small pore region rather than through the outer solvent layer. As the gap narrows the effective viscosity (at constant shear rate) begins to decrease again since the velocity of the upper plate (and hence the driving force for flow through the brush) decreases like λ (and thus faster than the pore size shrinks) at constant gap shear rate. It follows that the effective shear viscosity should decrease like $\lambda^{1/2}$ for small λ. These scalings will fail when compression comparable to the scale of the persistence length is induced.

In the recent simulations by Grest [3] and in the experiments by Klein *et al.* [2] the shear rate was not held constant but rather the *velocity* of the upper plate was kept constant. Thus the shear rate actually *increased* with decreasing gap. Our inset in Fig. 3(a) shows that under these conditions our simulations reproduce the *increasing* shear stress (increasing with decreasing gap like $\lambda^{-1/2}$ from the scaling arguments above) that are witnessed in both these studies.

Although the previous normal and shear force results are consistent with the experimental results presented by Klein *et al.* [2], they do not explain the remarkable features reported by Klein *et al.* [1] during high frequency oscillation. In the latter experiments, the normal forces increased dramatically at a critical oscillatory Weissenberg number. Such increases were not discovered in our steady simulations, and we turn to the dynamics of oscillatory flow to describe these experiments. We impose $u = U\cos(\omega t)$ at $y = b$ and follow the same simulation procedure with averages calculated at every time step.

A summary of our results for the normal forces and bead density profiles is given in Figs. 4 and 5 for oscillatory flow. We have shown calculations for a gap width $\lambda = 0.436$ (i.e., a brush which is compressed by about 50%), but similar results have been collected for a range of λ [18]. First, we have found that the dynamics of the brushes at large frequencies is markedly different than for lower frequency dynamics. In the high frequency regime the beads move with the fluid, and thus $\langle f_x \rangle \ll 1$, for almost the entire brush thickness. Moreover, because the total deformation of the brush in any cycle is small compared to its thickness, the brush never "feels" its tether, and the beads move affinely with the fluid. Thus the brush behaves more like a free suspension of spheres.

Since the beads are acting as if in free solution, the collisions of beads with their neighbors drives a normal motion of the brush analogous to "shear-induced diffusion" in the theory of free suspensions [19]. The collision process increases the fluctuating kinetic energy in the brush and causes the brush to diffuse from regions of high concentration to low [19]. In Fig. 5 we see the time-averaged brush density profiles at equilibrium and under oscillation at Wi = 570 at $\omega = 189$. The growth in the peak near the upward plate results from the diffusion process driving beads upward, and is located at

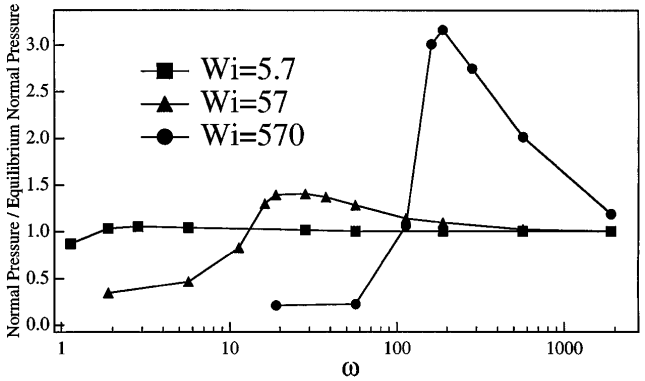

FIG. 4. Normal pressure versus frequency for oscillatory shear flow at $\lambda = 0.436$.

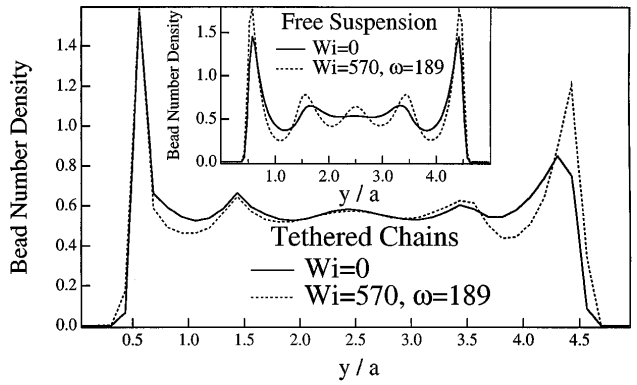

FIG. 5. Bead number density versus distance from tethered surface for oscillatory shear flow at $\lambda = 0.436$. The equilibrium brush density differs from Fig. 2 curve (a) because the brush is compressed. The inset shows the bead number density versus y/a for a suspension of free spheres in oscillatory shear flow at $\lambda = 0.436$.

a similar position as the peak in the density profile for a *sheared free suspension of spheres* (shown in the inset).

This shear-induced diffusion process and the resulting increase in bead concentration near the upper surface can result in greatly increased normal forces. In particular, we see in Fig. 4 that increases of nearly a factor of 3 in the normal force occur in a fairly narrow frequency range at large values of the Weissenberg number. These are comparable to the increases witnessed by Klein *et al.* [1]. If we assume a relaxation time for their brushes in the range of 0.01–0.001 s, then the range of Weissenberg number and dimensionless frequency for their experiments is 5–100 and 1.3–31, respectively, thus within the range of our simulated normal force increases.

The shear-induced diffusion process as it occurs in these brushes has other important characteristics. First, the frequencies must be such that the deformation of the brush is small compared to its characteristic thickness. Otherwise the brush will be significantly affected by the tether and no increase in bead density near the upper plate will occur. Also, the frequencies must be large such that the beads move affinely. Only in this case can the solvent penetrate the brush significantly and induce sufficient bead collisions throughout the brush—thus driving the diffusion process. We find that a maximum in the value of the normal forces occurs at $\mathrm{Wi}/\omega \approx 3$ and $\mathrm{Wi} \gg 1$. The ratio Wi/ω is independent of the chain relaxation time, and this suggests that we are resonating with the collision rate of the beads. In the experiments of Klein *et al.* [1] Wi/ω is in the range of 3.2–4.0.

Finally, this diffusion process should and does induce thickening in brushes which are not compressed by the upper wall. Indeed we have seen 1%–5% brush thickening in the right parameter regimes but only in the mean thickness of the brush—very few collisions occur in the "tails" of the brush and these are not thickened. We would expect to see increased thickening for longer polymers, since this would increase the rate of collisions that the chain experiences during the shearing process. Note that no brush thickening was ever witnessed in steady flow, and thus we find no evidence of the mechanisms given for brush thickening in the literature [9–11]. This shear-induced diffusion mechanism acts as an alternative, novel view of the shear-induced brush thickening.

The authors would like to thank the NSF Center for Polymers at Interfaces and Molecular Assemblies for supporting this work through Grant No. DMR-9400354-2. In addition, ESGS would like to thank the David and Lucile Packard foundation for additional support through Fellowship No. 91-3793.

[1] J. Klein, D. Perahia, and S. Warburg, Nature (London) **352**, 143 (1991).
[2] J. Klein, E. Kumacheva, D. Mahalu, D. Perahia, and L. J. Fetters, Nature (London) **370**, 634 (1994); J. Klein, E. Kumacheva, D. Perahia, D. Mahalu, and S. Warburg, Discuss Faraday Soc. **98**, 173 (1994).
[3] G. S. Grest, Phys. Rev. Lett. **76**, 4979 (1996); MRS Symposia Proceedings No. 264 (Materials Research Society, Pittsburgh, 1997).
[4] J. Klein, Y. Kamiyama, H. Yoshizawa, J. N. Israelachvili, G. H. Fredrickson, P. Pincus, and L. J. Fetters, Macromolecules **26**, 5552 (1993).
[5] D. H. Napper, *Polymeric Stabilization of Colloidal Dispersions* (Academic, London, 1983).
[6] Y. Inn and S.-Q. Wang, Phys. Rev. Lett. **76**, 467 (1996).
[7] S. T. Milner, Macromolecules **24**, 3704 (1988); Science **251**, 905 (1991).
[8] J. L. Anderson, P. F. McKenzie, and R. M. Webber, Langmuir **7**, 162 (1991).
[9] V. Kumaran, Macromolecules **26**, 2464 (1993).
[10] Y. Rabin and S. Alexander, Europhys. Lett. **13**, 49 (1990).
[11] J.-L. Barrat, Macromolecules **25**, 832 (1992).
[12] I. Neelov, O. Borisov, and K. Binder, (to be published).
[13] P. S. Doyle, E. S. G. Shaqfeh, and A. P. Gast, J. Fluid Mech. (to be published).
[14] H. A. Kramers, J. Chem. Phys. **14**, 415 (1944).
[15] J. D. Weeks, D. Chandler, and H. C. Anderson, J. Chem. Phys. **54**, 5237 (1971).
[16] D. L. Koch and J. F. Brady, AIChE J. **32**, 575 (1986).
[17] H. C. Brinkman, Appl. Sci. Res. **A1**, 27 (1947).
[18] P. S. Doyle, E. S. G. Shaqfeh, and A. P. Gast, Macromolecules (to be published).
[19] D. Leighton and A. Acrivos, J. Fluid Mech. **177**, 109 (1987); **181**, 415 (1987).